ORIGINAL ARTICLE

A transient thermal cloak experimentally realized through a rescaled diffusion equation with anisotropic thermal diffusivity

Yungui Ma[1], Lu Lan[1], Wei Jiang[1], Fei Sun[1,2] and Sailing He[1,2]

Transformation optics has made a major contribution to the advancement of modern electromagnetism and related research assisted by the development of metamaterials. In this work, we applied this concept to the thermodynamics using the coordinate transformation to the time-dependent heat diffusion equation to manipulate the heat flux by predefined diffusion paths. Experimentally, we demonstrated a transient thermal cloaking device engineered with effective thermal materials and successfully hid a centimeter-sized vacuum cavity. A rescaled heat equation accounting for all the pertinent parameters of various ingredient materials was proposed to greatly facilitate the fabrication. Our results unambiguously demonstrate the practical possibility of implementing complex transformed thermal media with high accuracy and acquiring several unprecedented thermodynamic functions, which we believe will help to broaden the current research and pave a new path to manipulate heat for novel device applications.

INTRODUCTION

Transformation optics (TO), a very powerful mathematical tool, has regained great interest in the research community since the pioneering works on electromagnetic (EM) cloaking independently performed by J Pendry and U Leonhardt.[1,2] Under the invariance of Maxwell's equations, the coordinate modification can transform virtual geometries into concrete physical EM media usually parameterized by anisotropic constants, enabling the manipulation of lights almost as arbitrarily as we desire. Excited by the tremendous application potential, great endeavors have been made to push EM cloaking toward practice in different spectra or dimensions.[1–8] The TO technique has also led to the creation of many other important EM devices with functionalities previously deemed impossible or unconceivable.[9–11] In general, this coordinate operation can be applied to different partial differential equations governing the behaviors of other physical phenomena such as thermal flux,[12–23] acoustic wave,[24–27] and matter or quantum[28–30] waves, demonstrating important scientific and application potentials.

Controlling heat diffusion with predefined paths has gained research interest in recent years for the potential device applications. In 2003, Greenleaf *et al.*,[31,32] initially worked out a mathematical problem of uniqueness for electrical conduction phenomena that was closely related to cloaking.[33] Later, these discussions led to the use of coordinate transformation to manipulate heat conduction.[12,13]

However, most of the previous discussions or thermal devices have been proposed by applying coordinate transformation to the thermostatic heat conduction equation,[12–14,19–21] that is, $\nabla \cdot (\kappa \nabla u) = 0$, with κ representing the thermal conductivity and u representing the temperature field. This approach limits the transformed devices to work only in a thermostatic state. For many practical applications, a device that can function in a transient state is more favorable or necessary to control the dynamic heat flux for specific purposes such as heat shielding[34] or energy harvesting.[35] This need requires addressing the general time-dependent heat diffusion equation, that is, $\rho c \cdot \partial u / \partial t = \nabla \cdot (\kappa \nabla u)$, where ρ and c are the density and the specific heat capacity of the medium, respectively.[15,16,18,22,23] This equation describes the heat diffusion in a solid out of the source region. Applying a coordinate mapping from the virtual (x, y) into the physical (x', y') spaces, Guenneau *et al.*[15] first derived the transformed medium that equally satisfied the heat equation

$$\rho' c' \frac{\partial u}{\partial t} = \nabla' \cdot (\boldsymbol{\kappa}' \nabla' u) \qquad (1)$$

with the new material parameters $\rho' c' = \rho c / \det(\boldsymbol{J})$ and $\boldsymbol{\kappa}' = \boldsymbol{J} \kappa \boldsymbol{J}^{\mathrm{T}} / \det(\boldsymbol{J})$, where $\boldsymbol{J}$ is the Jacobean matrix expressed by $\partial(x', y')/\partial(x, y)$. Later, by applying a transformation to Fick's equation, the same authors extended these discussions to more general scenarios, such as mass concentration diffusion.[16] It is clear that a device of transient

[1]Centre for Optical and Electromagnetic Research, JORCEP, State Key Lab of Modern Optical Instrumentation, Zhejiang University, Hangzhou, China and [2]Department of Electromagnetic Engineering, School of Electrical Engineering, Royal Institute of Technology, Stockholm, Sweden
Correspondence: Professor S He, Department of Electromagnetic Engineering, Royal Institute of Technology, Teknikringen 33, Floor 4, Room, Stockholm 100 44, Sweden.
E-mail: sailing@kth.se

response must account for the density and heat capacity as well as the anisotropic thermal conductivities, thus making it more challenging to implement. Very recently, in the preparation of current work,[36] such an attempt was reported by Schittny *et al.*[18] and showed a thermal cloak that was able to control the transient heat flux. In their design, two ingredient materials (copper and polydimethylsiloxane) with large thermal conductivity contrast were used to realize the anisotropic and inhomogenous conductivity profile by spatially adjusting their volume filling ratios. Unlike the previous static examples, which were similarly composed of two different materials,[14,19] Schittny's cloak was designed using a transient equation under the approximation of a constant $\rho'c'$, and the performance was improved by a numerically optimized background material. From a mathematical view, more ingredient materials are generally required to precisely execute Equation (1), which consists of four variables. Correspondingly, a different fabrication technique capable of subtly controlling the spatial composition is equally desired.

In this work, we simultaneously realized these complex parametric requirements (that is, $\rho'c' = const$ and anisotropic κ') using five different ingredient sheet materials, which offered the necessary freedoms to satisfy Equation (1) at different locations with theoretical approximation, and fabricated such a device exhibiting a prominent transient cloaking behavior. The manufacture efficiency of our device was mathematically improved by adopting a rescaled thermal equation and fully taking advantage of the abundance of natural materials with a wide range of thermal conductivity available from nearly zero to a value of >1000, which is impossible in the fabrication of EM devices.[3,9] Our work unambiguously proves the feasibility of extending EM TO devices into the thermal area and the robustness of the multilayer technique in fabricating complicated thermal devices, which may pave a new path to manipulate the dynamic heat flux for novel technological applications.

MATERIALS AND METHODS

For the simplicity of implementation, we discuss the transformation technique and its application in thermal devices in two dimensions (2D). Figures 1a and b present a schematic diagram of the creation of a thermal cloak using the transformation technique. Similar to the design of an EM cloak,[1–3] transformation allows us to expand a point in virtual space (Figure 1a) into a thermally invisible cavity in physical space (white region in Figure 1b), enclosed by an annular cloak (interior radius R_1 and exterior radius R_2). The heat flux is re-guided to flow around the cavity and restore their original diffusion paths outside the cloaking shell. As analyzed in Ref. 15 for an ideal thermal cloak, the heat energy requires an infinite time to pass through the innermost cloaking shell (which has nearly zero radial conductivity) before reaching the center cavity, thus offering thermal protection. However, in practice, we must use finite meshes in simulations or thin layers in experiments to approximate the continuous device with finite conductivity values. Thus,

the thermal energy will slightly diffuse into the inner cavity region and increase the temperature as the time elapses. This process is slower than that in the surrounding background, thus only offering a temporal heat protection. The same process occurs for a thermostatic cloak with the temperature inside the cloaking region being dependent on the spatial position where the transformation starts, as shown in Figure 1a.[14,17] Examples that demonstrate this behavior will be provided when discussing the simulation results in Figures 2a–l. Here, we would like to stress that a thermal cloak mainly acts as a flux-guiding shell to suppress the effect of a 'scatter' (thermal disturbance) in addition to the temporal thermal protection. One may introduce a thin, thermally insulating layer enclosing the cavity to improve the protection, as later indicated by our experiment in cloaking a vacuum cavity.

In our design and later fabrication, a simple linear coordinate mapping is selected to construct the material profiles of the thermal device, that is,

$$r = \frac{R_2 - R_0}{R_2 - R_1}r' - \frac{R_2(R_1 - R_0)}{R_2 - R_1}, \tag{2}$$

where r (r') is the radius in the virtual (physical) space. Here, we assume the expansion, as shown in Figure 1a, starts from a finite small region of radius R_0 ($= 0.005R_1$) rather than precisely from a point. This approximation on the initial condition leads to a negligible effect on the device performance but does reduce the demand on material parameters. In this work, our device is designed with $R_1 = 13$ mm and $R_2 = 20$ mm. Supplementary Figure S1 displays the transient cloaking behavior for the ideal case simulated by COMSOL. To implement such a device, one must discretize the continuous device and approximate it with many homogenous anisotropic concentric layers. In the limits of thermostatic circuitry, each anisotropic sub-layer can be approximated by many isotropic ingredient layers.[14,17] It is clear that at least four different ingredient layers are required to solve Equation (1), which has three unknowns, that is, $\rho'c'$ and the two principal values of anisotropic κ'. With the materials used in our experiment, as listed in Supplementary Table S1, we can mathematically fulfill the parametric requirements but only for a few sub-layers. To improve the fabrication efficiency, we modify the original equation by transferring $\rho'c'$ to the right side of Equation (1), that is,

$$\frac{\partial u}{\partial t} = \nabla' \cdot (\kappa'/\rho'c'\nabla'u) \tag{3}$$

We see the rescaled Equation (3) is effectively equivalent to Equation (1) if the condition $\nabla'(1/\rho'c') \approx 0$ is satisfied, which leads to $\nabla' \cdot (\kappa'/\rho'c'\nabla'u) = 1/\rho'c'\nabla' \cdot (\kappa'\nabla'u) + \kappa'\nabla'u \cdot \nabla'(1/\rho'c') \approx 1/\rho'c'\nabla' \cdot (\kappa'\nabla'u)$. This result sets up a precondition to use Equation (4) that the implemented device should have a nearly constant product of density and heat capacity across the sub-layers. With this condition satisfied, we now only need to implement the anisotropic thermal diffusivity $\alpha'(= \kappa'/\rho'c')$, which offers more freedom to select κ'. Note that a reduced conductivity was used in the first theoretical paper in Ref. 15 (see Eq. 18), which may worsen the impedance mismatch issue at the boundary. The transformed diffusivity profile in a cylindrical coordinate is calculated using

$$\alpha' = diag\{\frac{r}{r'}\frac{dr'}{dr}, \frac{r'}{r}\frac{dr}{dr'}, \frac{r}{r'}\frac{dr}{dr'}\}\alpha_0, \tag{4}$$

where α_0 is the diffusivity of the background. To implement this parametric profile defined by Equations (2) and (4), we discretized the device into seven
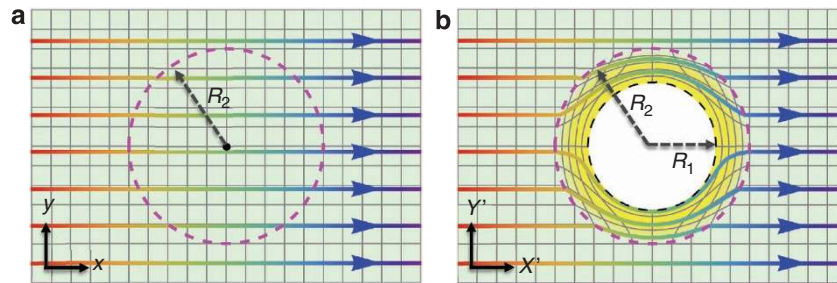

Figure 1 Schematic diagram of coordinate transformation for a thermal cloak. (**a**) The empty virtual space (x, y) and (**b**) the transformed physical space (x', y'). A simple linear coordinate transformation expands the central point in (**a**) into a white cavity enclosed by an annular cloaking shell (interior radius $\boldsymbol{R_1}$ and exterior radius $\boldsymbol{R_2}$). The colorful lines in the figures represent the diffusion trajectories of the heat flux.
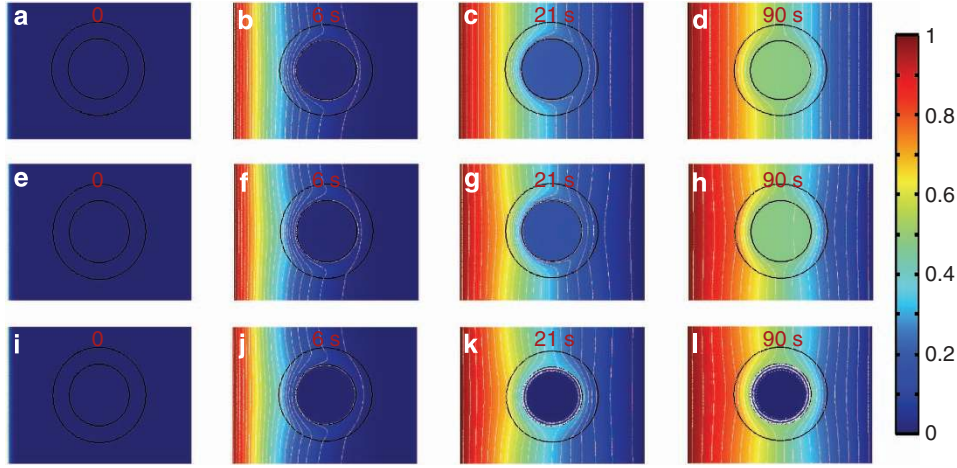
Figure 2 Simulated cloaking behavior. The first to fourth columns present snapshots of the normalized temperature distribution captured at $t = 0$, 6, 21 and 90 s, respectively. (**a–d**) The cases using an impedance-matched background ($\rho c = 2.1 \, \text{J cm}^{-3} \, \text{K}^{-1}$ and $\kappa = 71.4 \, \text{W m}^{-1} \, \text{K}^{-1}$) with the cloaking region filled by the same material as the background. The second (**e–h**) and the third (**i–l**) rows present the cases using the impedance-mismatched background of brass ($\text{Cu}_{70}\text{Zn}_{30}$, $\rho c = 2.1 \times 1.56 = 3.28 \, \text{J cm}^{-3} \, \text{K}^{-1}$ and $\kappa = 41.4 \times 1.56 = 111 \, \text{W m}^{-1} \, \text{K}^{-1}$) with the cloaking region occupied by a brass disk and a vacuum cavity, respectively. In the simulations, the heat flux originates from the left edge ($T_1 = 1$) and diffuses toward the right edge ($T_2 = 0$). The top and bottom edges are thermally isolated boundaries. The isothermal lines (orthogonal to the heat flux trajectories) are plotted in the white curves.

Table 1 Material parameters of thermal cloaking device

No.	Ti (%)	Al (%)	Cu (%)	p-G (%)	Ka (%)	$\overline{\rho'c'}$ (J cm^{-3} k^{-1})	$\overline{\alpha'_r}$ (mm^{-2} s^{-1})	$\overline{\alpha'_t}$ (mm^{-2} s^{-1})
1	–	–	0.1	0.84	0.05	1.22	1.71	623
2	–	–	0.50	0.49	0.012	2.19	3.4	277
3	–	0.7	–	0.28	0.007	2.00	6.16	199
4	0.7	–	–	0.35	–	1.94	7.9	151
5	0.6	0.2	–	0.25	–	2.08	9.0	121
6	0.5	0.4	–	0.18	–	2.19	10.7	105
7	0.43	0.4	–	0.14	–	2.22	11.3	99

Our cloaking device is composed of seven homogenous sub-layers. We used five different ingredient sheets to make the sub-layer, namely, titanium (Ti), aluminum (Al), copper (Cu), pyrolytic graphite (p-G) and kapton (Ka). The properties of these materials are provided in Supplementary Table S1. The volume percentage of each ingredient in each sub-layer is calculated using Equations (4) and (5). The right three columns list the averaged product ($\rho'c'$) of the density and heat capacity and the radial (α_r') and tangential (α_t') thermal conductivities designed for each sub-layer.

sub-layers, with each layer having an equal thickness of 1 mm, and engineered them with many thin ingredient sheets (their properties are given in Supplementary Table S1). The averaged parameters for each sub-layer are calculated using

$$\overline{\rho'c'} = \sum_{i=1}^{N} f_i \rho_i c_i, \quad \overline{\alpha'_r} = \left(\overline{\rho'c'} \sum_{i=1}^{N} \frac{f_i}{\kappa_i}\right)^{-1}, \quad \overline{\alpha'_t} = \sum_{i=1}^{N} f_i \kappa_i / \overline{\rho'c'}, \quad (5)$$

where ρ_i, c_i and κ_i are, respectively, the density, heat capacity and conductivity of the ith ingredient sheet whose volume ratio f_i satisfies $\sum_{i=1}^{N} f_i \approx 1$ (note that this approximation is made because each ingredient layer has finite thickness, and their summation may not be exactly unit). $\overline{\alpha'_r}$ and $\overline{\alpha'_t}$ are the averaged radial and tangential thermal diffusivities, respectively. Here, note that EM metamaterials are usually engineered with unit-cell sizes far smaller than the operating wavelength to validate the usage of effective medium theory.[37] For the thermal case, the ingredient materials composing the sub-layers should be selected with thicknesses as small as possible to achieve good accuracy in using the average

Equation (5) based on the analogy of a static thermal circuitry. Experimentally different ingredient sheets of thicknesses varying from 0.025 to 0.2 mm have been used to fabricate the 7-mm-thick cloaking shell, which has a total sheet number of 79. Details concerning the structural parameters and ingredient materials for each sub-layer are listed in Table 1, where we assume that the background has an isotropic diffusivity of $\alpha_0 = 34 \, \text{mm}^2 \, \text{s}^{-1}$. Note that the metals and pyrolytic graphite (with the largest anisotropic conductivity) used here provide good thermal stability for properties within the temperatures of interest from zero to $\sim 300 \, ^\circ\text{C}$,[38] which is very important for design and application. From Table 1, we see that the designed layers have roughly equal values of $\overline{\rho'c'}$ of $\sim 2.1 \, \text{J cm}^{-3} \, \text{K}^{-1}$, except for the first layer (that is, the innermost layer), which guarantees the rationality of using Equation (3). The parametric discrepancy of the first sub-layer does affect the overall cloaking performance, but not seriously, as numerically demonstrated in Figures 2a–l. This result is understandable because the sub-layer is very thin (1 mm), and the diffusivity is more decisive.

A great care has been taken to fabricate the samples. Our cloak shells consist of two equal halves that are separately manufactured and merged together later. During fabrication, we used the raw materials listed in Supplementary Table S1 to construct our device. The species and volume ratios of the ingredient sheets for each sub-layer are determined from Equation (5), which should also satisfy the requirement for a constant $\rho'c'$. The thicknesses of these ingredients in each sub-layer are determined with the aid of numerical simulations to confirm the validity of the static limit condition in using these averaged equations. For each sub-layer, we mix the different ingredient sheets as homogenously as possible by repeating their basic combination. Our implemented devices have a total of 79 layers of ingredient sheets. A compressive stress must be suitably applied in assembling these layers to produce a gapless sample without deformation. We used a $15 \, \text{cm} \times 10 \, \text{cm}$ rectangular brass board as the background material, which had 1.56 times larger ρc and κ than the thermal-impedance matched case (the matched ground has $\rho c = 2.1 \, \text{J cm}^{-3} \, \text{K}^{-1}$ and $\kappa = 34 \times 2.1 = 71.4 \, \text{W m}^{-1} \, \text{K}^{-1}$). This reduction does diminish the cloaking performance, as numerically demonstrated in Figures 2e–l.

Our measurement was conducted in a vacuum chamber with an infrared window on top to measure the radiated infrared light that is associated with the temperature field of the sample by Planck thermal emission. Rather than a constant temperature source, as used in the simulation, we used a 40-W strip heater glued on the left edge of the brass with silicon grease to produce the heat and submerged the right edge in an ice-water sink to attenuate the heat. The

evolution of the temperature field was captured by a Mikron 7500l infrared camera (Mikron Infrared Inc., Oakland, NJ, USA), with a time interval of 1.5 s between successive shots. The vacuum pressure in the measurement was maintained below 2 Pa. The thermal emission efficiency of the sample was improved by spraying an ~20-μm thick layer of blackbody paint (Okitsumo Incorporated, Nabari city, Japan) on the top surface of the sample, whose effect on the thermal diffusion of the sample could be neglected. Our set-up allows the measurement of 2D thermal diffusion behavior, as required by our design. A photograph of our measurement set-up is provided in Supplementary Figure S2.

RESULTS

Simulation results

We first describe the simulation results of transient heat cloaking using COMSOL. Figures 2a–d present four snapshots of the temperature field image captured at time $t = 0$, 3, 21 and 90 s, for the device defined by the parameters given in Table 1. In the simulation, we used the normalized constant temperature as the left ($T_1 = 1$) and right ($T_2 = 0$) boundaries and the thermal insulation for the top and bottom boundaries. For the first example, the background and cloaking region are filled by the same material, with $\rho c = 2.1$ J cm^{-3} K^{-1} and $\kappa = 34 \times 2.1 = 71.4$ W m^{-1} K^{-1}. As indicated by the white isothermal lines, the heat flux flows around the cloaked region and restores their straight diffusion trajectories (orthogonal to the isothermal lines) after passing through the region. The temperature field outside the cloak is only slightly disturbed, as if no disturbance exists in the flux paths. We also observe the slow increase in the temperature inside the cloaked region as time elapses, with the reasoning addressed earlier. At $t = 90$ s, the thermal system almost reaches the equilibrium state, and the temperature field mimics the ideal case (Supplementary Figure S1). These snapshots and their close match with the ideal case justify the approximations made to rescale the thermal equation and homogenize the continuous profile with multiple layers in the process of implementation. In the experiment, we use brass (Cu$_{70}$Zn$_{30}$) as the background material, whose values of both ρc and κ are 1.56 times larger than those used in the above simulation (that is, the diffusivity is the same). This reduced

background will lead to a thermal impedance ($\propto 1/\kappa$ in the static limit) mismatch at the device's exterior boundary and degrade the cloaking performance by causing a weak 'shadow' after the cloak, as shown in Figures 2e–l. It is similar to the rescaling measure adopted in the EM cloaks to acquire a constant tangential permeability.[3,9,39] We make this sacrifice to conduct the experiment with available materials and in a reasonable measuring period. Figures 2i–l present snapshots of the temperature field with the cloaking region replaced by a vacuum cavity, an absolute 'scatter', which will behave similarly to the perfectly electric conducting metal used in an EM cloak.[3,4] In this case, no energy will diffuse into the center region. Almost no differences are observed in the temperature field compared with those shown in the second row of Figure 2, indicating the robust cloaking performance of our designed devices, that is, insensitivity to the materials placed inside the cloaking region.

Measurement results

Figure 3a presents a photograph of a fabricated thermal cloak consisting of 79 ingredient sheets. The quality of the device, in particular, the effect of the thermal interface resistance between sheets, must be experimentally examined. Figure 3b displays the anisotropic diffusivity values of each sub-layer with the lines calculated by Equation (5) and the symbols from Table 1. We implemented the device with the effective parameters (for effective realization) as close as possible to the theoretical values by carefully selecting the ingredient sheets (species and thickness) that simultaneously satisfied $\rho' c' =$ constant for most of the layers. This step is generally accomplished using multiple ingredient materials for each sheet. Figure 3c presents a schematic diagram of our experimental set-up conducted in a vacuum environment. Here, we used an infrared camera to capture the temperature field of the sample through Planck thermal emission. More details about the sample fabrication and measurements are provided in Materials and methods. In our experiment, we fabricated two cloak samples, with one having a brass center and the other having a vacuum cavity in the cloaking region. For reference, we also measured the temperature field of similarly sized bare brass.
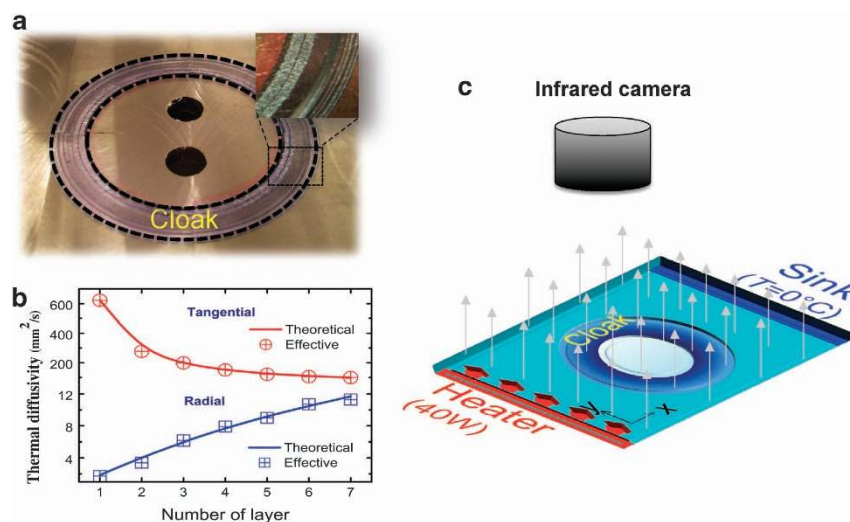

Figure 3 Device and measurement. (**a**) A photo of a fabricated cloaking device. The cloak shell is highlighted by two dashed lines. The inset in (**a**) provides a zoomed-in image of part of the cloak shell. (**b**) The tangential (top) and radial (bottom) thermal diffusivities of different sub-layers. The solid lines represent the theoretical values calculated using Equation (4), and the symbols represent the effective values designed for each sub-layer using Equation (5). (**c**) Schematic diagram of our measurement set-up in vacuum. A 40-W strip heater source is glued to the left edge of the brass, and an ice-water sink is used at the right edge to induce the heat flux. The other boundaries in the vacuum mimic thermal insulation conditions, which are consistent with the simulation. The evolution of the temperature field is captured by an infrared camera at a time interval of 1.5 s.

Figure 4a presents a photograph of rectangular bare brass, and Figures 4b–d illustrate its transient conduction behavior with the temperature snapshots that were captured 2, 6 and 15 min after switching on the power of the heater, respectively. The isothermal lines are plotted in the white curves. An animation movie with additional photos is provided in Supplementary Movie 1. A nearly ideal planar temperature front, indicating a straight heat flux, is observed for the empty background. Note that our measurement period is far larger than that used in the simulation, as the constant-power source used here requires a long time (~ 13 min) to reach thermal equilibrium. However, this difference will not affect our evaluation of the samples' performances referring to the simulation results. Figure 4e presents an image of our first sample for cloaking a brass disk. The two small holes in the disk are left during the manufacture. Figures 4f–h present snapshots of the temperature field captured at $t = 2$, 6 and 15 min, respectively. Additional photos for an animation movie are provided in Supplementary Movie 2. From the isothermal lines, we observe that the heat flux (orthogonal to the isothermals) is guided to flow around the center disk and diffuse forward with little disturbance compared with the top figures for a bare background. The brass disk has a nearly uniform temperature profile that increases slowly with absolute values much smaller than those in the left surrounding medium. This transient behavior is consistent with the numerical predictions in Figures 2e–h.

Figure 4i presents a photograph of our second cloak sample with a cavity hole (radius $= 9$ mm) in the cloaking center. Note that here we used a 4-mm-thick brass ring to support the cloak shell. Figures 4j–l present snapshots of the temperature field captured at 2, 6 and 15 min, respectively. An animation is provided in Supplementary Movie 3. Assisted by the isothermal line, these figures demonstrate that the heat flux is guided around the cavity and restores their diffusion direction after the cloak. The strong 'scatter' (thermal disturbance) has a slight effect on the heat flux and the temperature field, as indicated by the slightly more distorted isothermal lines after the cloak compared with Figures 4g and h, with a solid brass disk in the cloaking region. The experimental results agree well with the simulations presented in Figures 2i–l. We should emphasize that the distortion of the isothermal lines near the sample is mainly caused by the thermal impedance mismatch between the device and the background, as addressed in our previous analysis, although a vacuum cavity of the same size without cloaks could induce a similar distorted near-field temperature profile. Evidence of this phenomenon is provided in the simulations (see Figures 2c and d), which demonstrate that the straight wavefront of the isothermal lines is restored right after the cloak for the matched case. A similar cloaking effect was observed in a recent experiment by another group, where an optimization program was used to achieve matched boundary parameters.[18] Note that our experimental results in Figure 4l agree well with the simulation results of Figure 2l for an impedance-mismatched case (a vacuum cavity with the cloak). Thus, we conclude that the sample fabricated here using multilayers did behave as a cloaking shell that can guide the heat flux without disturbing the enclosed vacuum cavity.

DISCUSSION

In this work, we have implemented a coordinate-transformed thermal device and demonstrated its transient thermal cloaking behavior. To facilitate the fabrication, we adopted the rescaled thermal diffusion equation and used the anisotropic thermal diffusivity (instead of the thermal conductivity used in the literature) as the key parameter for the design. This treatment is fundamentally different from a thermo-static case, where only conductivity is considered and is practically validated by satisfying the prerequisite for the product of the density and heat capacity and is intrinsically consistent with the general time-dependent thermal equation. The strict requirements on the material parameters in our design are deliberately fulfilled by selecting appropriate multiple ingredient layers rather than the two alternating layers used for the static device.[14,17] The machining and assembly of the devices must be carefully conducted; otherwise, defects such as thermal interface resistance will be induced, which may easily damage the final parametric profile and, consequently, the sample performance. Our experimental results explicitly demonstrate the possibility of fabricating such a complex sample with engineered thermal metamaterials. Unlike the EM metamaterials designed for
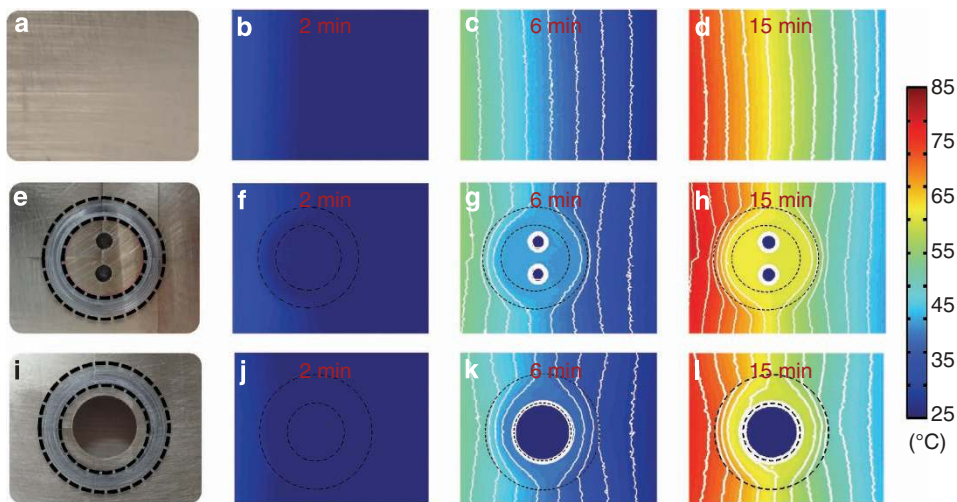

Figure 4 Samples and measured temperature field. (**a**) A top view of the rectangular bare brass. (**b–d**) Corresponding snapshots of the temperature field captured at $t = 2$, 6 and 15 min, respectively, for the bare brass background. (**e**) A top view of the cloaking device with a brass disk in the cloaking region. The two small holes are left in the manufacture. (**f–h**) Corresponding snapshots of the temperature field captured at $t = 2$, 6 and 15 min, respectively, for this sample. (**i**) A top view of the cloaking device with a vacuum cavity in the cloaking region. (**j–l**) Corresponding snapshots of the temperature field captured at $t = 2$, 6 and 15 min, respectively, for this sample. The isothermal lines (orthogonal to the heat flux trajectories) are drawn in white. Animations illustrating the evolution of the temperature field are shown in Supplementary Movies 1–3.

transformed wave devices, which are usually highly dispersive and offer narrow band response,[3] thermal metamaterials and the implemented devices can be fabricated using natural materials and are, thus, more promising and robust in practice. The temperature issue could be solved by controlling the ingredient species and the temperature window for application.

TO has issued a major advancement in modern EM research by producing many fascinating EM devices that were previously unconceivable or deemed impossible. We may also believe that transformation thermodynamics can lead to revolutionary thermal technologies or devices through the precise manipulation of the heat flux. Applications can be envisioned such as transformed devices to improve the efficiencies of energy harvesting for thermoelectrics by creating low thermal and high electric conductivity profiles[35] or to fulfill a specific heat flux channel for a thermal circuit.[40] Transformation thermodynamics may also provide unique methods to solve problems in heat management encountered by a chip designer,[34] for example, the construction of a specific substrate or embedding of a medium to guide away the heat. We may also integrate TO and thermodynamics in a single device to achieve simultaneous manipulation of both light and heat that can be excited for thermal-optical applications such as thermal photovoltaic devices.[41]

CONFLICT OF INTEREST

The authors declare no conflict of interest.

1 Pendry, J., Schurig, D. & Smith, D. R. Controlling electromagnetic fields. *Science* **312**, 1780–1782 (2006).
2 Leonhardt, U. Optical conformal mapping. *Science* **312**, 1779–1780 (2006).
3 Schurig, D., Mock, J. J., Justice, B. J., Cummer, S. A., Pendry, J. B., Starr, A. F. & Smith, D. R. Metamaterial electromagnetic cloak at microwave frequencies. *Science* **324**, 977–980 (2006).
4 Liu, R., Chettiar, U. K., Kildishev, A. V. & Shalaev, V. M. Broadband ground-plane cloak. *Science* **323**, 366–369 (2009).
5 Valentine, J., Li, J. S., Zentgraf, T., Bartal, G. & Zhang, X. An optical cloak made of dielectrics. *Nat. Mater.* **8**, 568–571 (2009).
6 Ergin, T., Stenger, N., Brenner, P., Pendry, J. B. & Wegener, M. Three-dimensional invisibility cloak at optical wavelengths. *Science* **328**, 337–339 (2010).
7 Zhou, F., Bao, Y. J., Cao, W., Stuart, C. T., Gu, J. Q., Zhang, W. L. & Sun, C. Hiding a realistic object using a broadband terahertz invisibility cloak. *Sci. Rep.* **1**, 78 (2011).
8 Ma, H. F. & Cui, T. J. Three-dimensional broadband ground-plane cloak made of metamaterials. *Nat. Commun.* **1**, 124 (2011).
9 Ma, Y. G., Ong, C. K., Tyc, T. & Leonhardt, U. An omnidirectional retroreflector based on the transmutation of dielectric singularities. *Nat. Mater.* **8**, 639–642 (2009).
10 Chen, H. Y., Chan, C. T. & Sheng, P. Transformation optics and metamaterials. *Nat. Mater.* **9**, 387–396 (2010).
11 Lai, Y., Chen, H., Zhang, Z. Q. & Chan, C. T. Complementary media invisibility cloak that cloaks objects at a distance outside the cloaking shell. *Phys. Rev. Lett.* **102**, 93901 (2009).

12 Fan, C., Gao, Y. & Huang, J. Shaped graded materials with an apparent negative thermal conductivity. *Appl. Phys. Lett.* **92**, 251907 (2008).
13 Chen, T., Weng, C. N. & Chen, J. S. Cloak for curvilinearly anisotropic media in conduction. *Appl. Phys. Lett.* **93**, 114103 (2008).
14 Narayana, S. & Sato, Y. Heat flux manipulation with engineered thermal materials. *Phys. Rev. Lett.* **108**, 214303 (2012).
15 Guenneau, S., Amra, C. & Veynante, D. Transformation therdyamics: cloaking and concentrating heat flux. *Opt. Express* **20**, 8207–8218 (2012).
16 Guenneau, S. & Puvirajesinghe, T. M. Fick's second law transformed: one path to cloaking in mass diffusion. *J. R. Soc. Interface* **10**, 20130106 (2013).
17 Han, T. C., Yuan, T., Li, B. W. & Qiu, C. W. Homogeneous thermal cloak with constant conductivity and tunable heat localization. *Sci. Rep.* **3**, 1593 (2013).
18 Schittny, R., Kadic, M., Guenneau, S. & Wegener, M. Experiments on transformation thermodynamics: molding the flow of heat. *Phys. Rev. Lett.* **110**, 195901 (2013).
19 Xu, H. Y., Shi, X. H., Gao, F., Sun, H. D. & Zhang, B. L. Experimental demonstration of an ultra-thin three-dimensional thermal cloak. arXiv:1306.6835.
20 Han, T., Bai, X., Thong, J. L., Li, B. & Qiu, C.-W. Bilayer isotropic thermal cloak. arXiv:1307.2507.
21 Han, T., Zhao, J., Yuan, T., Lei, D. Y., Li, B. & Qiu, C. W. Theoretical realization of an ultra-efficient thermal-energy harvesting cell made of natural materials. *Energy Environ. Sci.* doi:10.1039/c3ee41512k .
22 Narayana, S., Savo, S. & Sato, Y. Transient heat flux shielding using thermal metamaterials. *Appl. Phys. Lett.* **102**, 201904 (2013).
23 Guenneau, S. & Amra, C. Anisotropic conductivity rotates heat fluxes in transient regimes. *Opt. Express* **21**, 6578 (2013).
24 Cummer, S. A. & Schurig, D. One path to acoustic cloaking. *New J. Phys.* **9**, 45 (2007).
25 Chen, H. Y. & Chan, C. T. Acoustic cloaking in three dimensions using acoustic metamaterials. *Appl. Phys. Lett.* **91**, 183518 (2007).
26 Zhang, S., Xia, C. & Fang, N. Broadband acoustic cloak for ultrasound waves. *Phys. Rev. Lett.* **106**, 024301 (2011).
27 Sanchis, L., García-Chocano, V. M., Llopis-Pontiveros, R., Climente, A., Martínez-Pastor, J., Cervera, F. & Sánchez-Dehesa, J. Three-dimensional axisymmetric cloak based on the cancellation of acoustic scattering from a sphere. *Phys. Rev. Lett.* **110**, 124301 (2013).
28 Milton, G. W., Briance, M. & Willis, J. R. On cloaking for elasticity and physical equations with a transformation invariant form. *New J. Phys.* **8**, 248 (2006).
29 Zhang, S., Genov, D. A., Sun, C. & Zhang, X. Cloaking of matter waves. *Phys. Rev. Lett.* **100**, 123002 (2008).
30 Greenleaf, A., Kurylev, Y., Lassas, M., Leonhardt, U. & Uhlmann, G. Cloaked electromagnetic, acoustic, and quantum amplifiers *via* transformation optics. *PNAS* **109**, 10169–10174 (2012).
31 Greenleaf, A., Lassas, M. & Uhlmann, G. Anisotropic conductivities that cannot be detected by EIT. *Physiol. Meas.* **24**, 413 (2003).
32 Greenleaf, A., Lassas, M. & Uhlmann, G. On nonuniqueness for Calderon's inverse problem. *Math. Res. Lett.* **10**, 685–693 (2003).
33 Greenleaf, A., Kurylev, Y., Lassas, M. & Uhlmann, G. Invisibility and inverse problems. *Bull. Am. Math. Soc.* **46**, 55–97 (2009).
34 Yan, Z., Liu, G. X., Khan, J. & Balandin, A. A. Graphene quilts for thermal management of high-power GaN transistors. *Nat. Commun.* **3**, 827 (2012).
35 Leclerc, M. & Najari, A. Organic thermoelectrics: green energy from a blue polymer. *Nat. Mater.* **10**, 409–410 (2011).
36 Leonhardt, U. Cloaking of heat. *Nature* **498**, 440–441 (2013).
37 Koschny, T., Kafesaki, M., Economou, E. N. & Soukoulis, C. M. Effective medium theory of left-handed materials. *Phys. Rev. Lett.* **93**, 107402 (2004).
38 Madelung, O. & White, G. K. *Thermal Conductivity of Pure Metals and Alloys* 6–106 (Springer-Verlag, Berlin Heidelberg, 1991).
39 Cummer, S. A., Popa, B.-I., Schurig, D., Smith, D. R. & Pendry, J. B. Full-wave simulations of electromagnetic cloaking structures. *Phys. Rev. E* **74**, 036621 (2006).
40 Li, N. B., Ren, J., Wang, L., Zhang, G., Hänggi, P. & Li, B. W. Phononics: Manipulating heat flow with electronic analogs and beyond. *Rev. Mod. Phys.* **84**, 1045–1066 (2012).
41 Schwede, J. W., Bargatin, I., Riley, D. C., Hardin, B. E., Rosenthal, S. J., Sun, Y., Schmitt, F., Pianetta, P., Howe, R. T., Shen, Z. X. & Melosh, N. A. Photon-enhanced thermionic emission for solar concentrator systems. *Nat. Mater.* **9**, 762–767 (2010).

Supplementary Information accompanies the paper on the NPG Asia Materials website (http://www.nature.com/am)